Controlled growth of CNT in mesoporous AAO through optimized conditions for membrane preparation and CVD operation

Paolo Ciambelli, Laurent Arurault, Maria Sarno, Sandra Fontorbes, Caterina Leone, Lucien Datas, Diana Sannino, Pascal Lenormand, S. Le Blond Du Plouy

doi:10.1088/0957-4484/22/26/265613

Controlled growth of CNT in mesoporous AAO through optimized conditions for membrane preparation and CVD operation

P Ciambelli[1,2], L Arurault[3], M Sarno[1,2], S Fontorbes[3], C Leone[1,2], L Datas[3], D Sannino[1,2], P Lenormand[3] and S Le Blond Du Plouy[3]

[1] Department of Chemical and Food Engineering, University of Salerno, I-84084 Fisciano (SA), Italy

[2] Centre NANO_MATES, University of Salerno, I-84084 Fisciano (SA), Italy

[3] Université de Toulouse, CIRIMAT, UPS/INPT/CNRS, LCMIE, F-31062 Toulouse Cedex 9, France

E-mail: msarno@unisa.it and arurault@chimie.ups-tlse.fr

Abstract

Anodic aluminium oxide (RAAO) membranes with a mesoporous structure were prepared under strictly controlling experimental process conditions, and physically and chemically characterized by a wide range of experimental techniques. Commercial anodic aluminium oxide (CAAO) membranes were also investigated for comparison. We demonstrated that RAAO membranes have lower content of both water and phosphorus and showed better porosity shape than CAAO. The RAAO membranes were used for template growth of carbon nanotubes (CNT) inside its pores by ethylene chemical vapour deposition (CVD) in the absence of a catalyst. A composite material, containing one nanotube for each channel, having the same length as the membrane thickness and an external diameter close to the diameter of the membrane holes, was obtained. Yield, selectivity and quality of CNTs in terms of diameter, length and arrangement (i.e. number of tubes for each channel) were optimized by investigating the effect of changing the experimental conditions for the CVD process. We showed that upon thermal treatment RAAO membranes were made up of crystallized allotropic alumina phases, which govern the subsequent CNT growth, because of their catalytic activity, likely due to their Lewis acidity. The strict control of experimental conditions for membrane preparation and CNT growth allowed us to enhance the carbon structural order, which is a critical requisite for CNT application as a substitute for copper in novel nano-interconnects.

1. Introduction

Carbon nanotubes (CNTs) and nanofibres (CNFs) have drawn more and more attention due to their unique physical characteristics and the subsequent wide range of possible applications (electrical, mechanical, etc). However, for most of these applications, well-controlled characteristics (diameter, length, density, order, degree of purity) of the carbon nano-objects are required [1–6]. One of the usual methods to achieve the tuning and vertical alignment of CNTs is the use of ordered meso-or microstructured anodic aluminium oxide (AAO) as the templating matrix. Previous works mainly used commercial AAO (CAAO) membranes [7–16] or research AAO (RAAO) templates, usually prepared by anodization [1, 4, 7] performed in a sulfuric, oxalic or phosphoric acid electrolyte. The RAAO templates were either through-pores membranes or AAO structures supported on a coated Si substrate [17, 18]. In most studies the growth of

CNTs or CNFs was catalytically promoted by metal particles (usually Co) electrochemically deposited at the pore bottom of the pores [19–25], while a smaller number of papers [7–16] reported carbon pyrolysis without a catalyst. In all these previous works the AAO templates were generally considered as inert structures made up of crystallized alumina (Al_2O_3), without any impact on the carbon growth, while different papers [13, 26–30] reported that the pore internal surface of the AAO template can itself play a catalytic role for the decomposition of hydrocarbons. However, they did not identify the surface active sites.

It has been proposed [31] that the Lewis acid surface sites present in amorphous and transition alumina have an intrinsic catalytic activity in the decomposition and recombination of unsaturated carbon.

Recently, Al_2O_3 and other unusual catalysts [32–34] have been found able to grow single-walled carbon nanotubes (SWNTs). However, Haung *et al* conclude that the growth is due to the catalyst nanosize [32]. Homma *et al* [33] proposed a new mechanism for the growth of SWNTs (in addition to the vapour–liquid–solid (VLS) growth mechanism for metals), passing through the formation of a carbon film on the nanoparticles, with the generation of a five-membered ring graphene island acting as a nucleus for SWNT growth. However, SWNTs can grow also on nanosized protrusions on the surface of large Al_2O_3 particles [34]. Therefore, the mechanism of CNT growth in the channels of an AAO membrane, without using a metal catalyst, has not yet been elucidated.

Nevertheless, it is well known that template CNTs not catalytically grown [1, 7–9, 11–13, 18] have open tips, a well-formed central hole and are very pure. However, the tube walls are not so graphitized, requiring thermal annealing at very high temperature [7, 35, 36] to obtain graphitized carbon. On the other hand, a change in the less expensive operating conditions can affect the tube quality, too. Despite the number of papers present in the literature, only in a few cases is a screening of process parameters [13, 37] reported. In particular, as far as we are aware, neither the effect of all growth parameters such as temperature, total feed flow, partial pressure of carbon precursor, reaction time and carbon feedstock, nor an accurate comparison of commercial (CAAO) and synthesized membranes (RAAO) as growth templates have been reported [1, 5, 7–9, 13, 38].

Hornyak *et al* [37] explored the temperature effect on the graphitic character of CNTs, finding that it improved significantly as CVD temperature was increased from 500 to 800 °C: the samples showed a progressive enhancement of both metallic appearance and layered tube wall structure and decrease of electrical resistance. No significant enhancement of graphitization was observable under microscopic and Raman spectroscopy investigations, among samples formed at 800, 900 and 1000 °C, even if a further decrease in the electrical resistivity was observed under this temperature increase.

The aim of the present study was to prepare ordered CNTs in CAAO and RAAO mesoporous membranes, by controlling the synthesis parameters in order to accurately tune carbon nanotube characteristics in terms of diameter, length and arrangement (i.e. number of tubes for each channel). The CNTs were produced by chemical vapour deposition (CVD) in the absence of a catalyst and in different experimental conditions that were correlated with the quality of the carbon materials obtained. A wide range of microscopic observations (FEG-SEM, SEM, TEM) and physico-chemical characterizations (IRS, XRD, EPMA, TGA-DTGA) were performed on AAO templates, AAO/CNT composites and CNTs after membrane dissolution, in order to especially highlight the chemical composition of the AAO template and the CNT characteristics under the different growth conditions.

2. Experimental details

2.1. Preparation process of the AAO membranes

The preparation process of the anodic aluminium oxide (AAO) porous templates was extensively described elsewhere [39, 40], but these previous works were mainly focused on the preparation of porous AAO ordered films still including the compact layer and sometimes supported on the metallic substrate, while the present study deals with the AAO membranes, i.e. through-pores templates.

The aluminium substrate ($Ø_{sample}$ = 14 mm) was prepared first by sanding and then by annealing under nitrogen atmosphere at 450 °C for 2 h. Additional electropolishing was carried out at 25 V for 2 min in a Jacquet mixed solution.

Anodization was carried out without delay at 185 V for 4 h. The electrolyte was made up of a vigorously mixed aqueous phosphoric acid solution (8 wt%), while a pure aluminium plate was used as the cathode. The temperature was regulated at −1.5 °C by a cryostat (Huber CC2), and the voltage was applied by an Invensys Lambda generator (300 V, 5 A).

Specifically in the present study, after growth of the porous anodic film, an additional removal of the compact layer was performed using 30 V AC voltage (Universal Power Supply EA-4036) in a phosphoric acid solution (16 wt%) and the aluminium substrate was chemically dissolved with a hydrochloric acid solution (18 wt%) including copper chloride CuCl (0.1 mol l^{-1}). The membrane was dipped for 5 min in a phosphoric acid solution (8 wt%) and finally rinsed with deionized water.

All chemical compounds used for all steps of this preparation process were analytical grade and aqueous electrolyte solutions were obtained using deionized water. The prepared research membrane was called RAAO in the following.

As a comparison, commercial membranes (Anodisc; sample diameter:13 mm; pore diameter: 0.2 mm) manufactured by Whatmann were also studied (CAAO).

2.2. Microscopic and chemical analysis of the AAO membranes

A field emission gun scanning electron microscope (FEG-SEM JEOL JSM 6700F) was used to determine the morphology of the pores, i.e. the pore density (ρ), the pore diameter (d_p),

Table 1. CNT operational conditions.

Sample	Reaction temperature (°C)	Reaction time (min)	Total feed flow (cm^3(stp) min^{-1})	C_2H_4 (vol.%)	Membrane type
M29	850	30	100	10	RAAO
M30	850	30	100	10	CAAO
M31	850	10	100	10	CAAO
M34	850	10	100	10	RAAO
M32	850	10	100	5	CAAO
M60	950	30	100	10	CAAO
M61	950	30	200	5	CAAO
M78	970	30	200	3	CAAO
M81	950	30	200	3	CAAO
M144	950	30	200	3	RAAO

the thickness of the porous layer (e_p), the percentage of the void volume (τ) and the interdistance between the edge of two adjacent pores.

X-ray diffraction (XRD) analysis was performed with a Bruker AXS D4 Endeavor generator with copper anticathode ($K_\alpha = 1.5418$ Å). All diffraction profiles were obtained by varying 2θ from 10° to 100°. Finally, peaks were identified by EVA software.

The coating dehydration and crystallization processes were studied by thermogravimetric analysis (TGA) in nitrogen 4.5 from 25 to 900 °C at a heating rate of 10 °C min^{-1}, by using a SETARAM instrument (Model TAG 92 equipped with a platinum crucible).

The infrared spectroscopy (IRS) was performed using an IR-TF Nicolet 510P instrument, the spectra being recorded in transmission conditions between 400 and 4000 cm^{-1}. The anodic films were preliminarily reduced to powder and prepared in KBr pellets.

The quantitative elemental chemical analysis was carried out using an Electron Probe MicroAnalyser (EPMA—CAMECA SX50). Eight measurements were made on the whole sample surface.

2.3. Process of carbon nanotube growth

Carbon nanotubes were synthesized by chemical vapour deposition (CVD) of ethylene within the pores of both RAAO and CAAO membranes. Hydrocarbon pyrolysis was carried out in a laboratory apparatus consisting of a continuous flow microreactor, fed by an ethylene–nitrogen gas mixture [11, 12]. For each gas a mass flow controller (MFC) was used in order to ensure a constant and controlled flow rate.

A set of experiments have been conducted on commercial membranes to find the optimal synthesis conditions by varying (table 1): temperature, ethylene feed concentration, reaction times, with respect to the quality of the materials obtained. The syntheses have been performed in isothermal conditions after a pretreatment of the membrane under nitrogen flow, from room temperature up to the synthesis temperature.

The recovery of carbon material was performed by treating a fraction of carbon-loaded membrane samples for 24 h with 20 ml of 50 wt% HF aqueous solution to dissolve the membrane; the solid residue was washed in distilled water, centrifuged and finally dried at 353 K for 12 h.

2.4. Characterization of AAO membrane–carbon composite and of recovered carbon nanotubes

The samples after synthesis and the recovered carbon nanotubes were characterized using various techniques. Scanning electron microscopy (SEM) pictures were obtained with a LEO 1525.

Transmission electron microscopy (TEM) images were obtained with a JEOL 1200 EX2 microscope. The accelerating voltage of the electron beam was 200 kV. The samples were mounted on a Quantifoil® microgrid carbon polymer supported on a copper grid by dropping the sample suspension, obtained after a few minutes of sonication, onto the grid. The microscope was equipped with an energy-dispersive x-ray spectroscopy (EDX) probe (probe size 1.5 nm).

Simultaneous thermogravimetric and differential thermal analysis (TG–DTG) was performed with a Thermogravimetric Analyser SDTQ 500 (TA Instruments). The measurements were performed in the range 25–900 °C, with a 10 °C min^{-1} heating rate under flowing air.

Raman spectra were obtained at room temperature with a micro-Raman spectrometer Renishaw inVia (514 nm laser excitation wavelength).

3. Results and discussion

The AAO membranes were characterized, before the CNT growth, in order to know their microstructure and chemical composition just at the end of the preparation process but also after a thermal treatment. The results were systematically compared with those obtained using the Whatmann commercial membranes.

3.1. Microstructural characterizations of the AAO membranes

3.1.1. Commercial membranes. Whatmann commercial membranes have often been used for the growth of carbon nanotubes [7, 9–11], but surprisingly they remain poorly studied. They were usually considered as through-pores membranes, showing two identical faces and made up of inert and crystallized alumina Al_2O_3.

Yet FEG-SEM cross-sectional views (figures 1(a) and (b)) showed that pores are indeed opened on both sides but that the two opposite porosities are significantly different. In particular, one side, rarely shown, is quite complex and

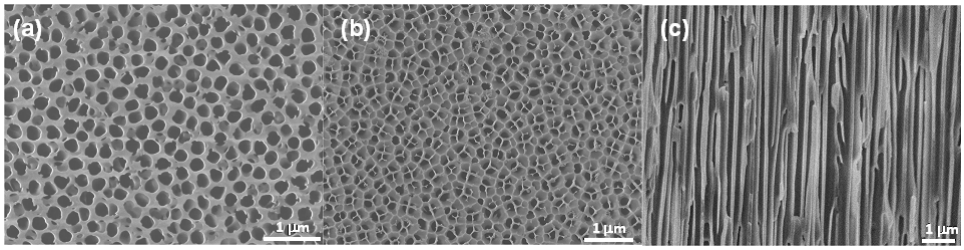

Figure 1. FEG-SEM views of the CAAO membrane: (a) side A, (b) side B and (c) cross section.

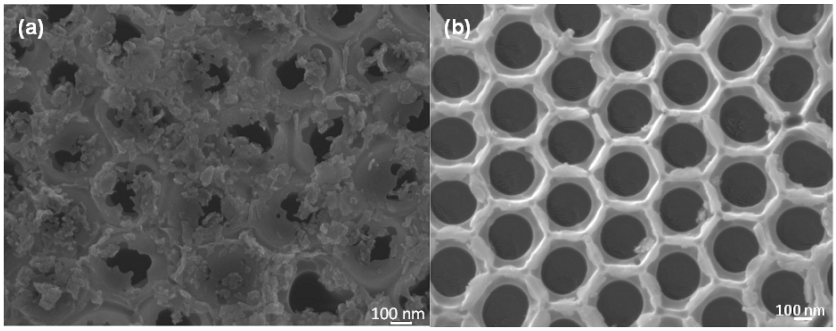

Figure 2. FEG-SEM cross-sectional views of the RAAO membrane at different durations of the removal of the compact layer: (a) 30 min and (b) 40 min.

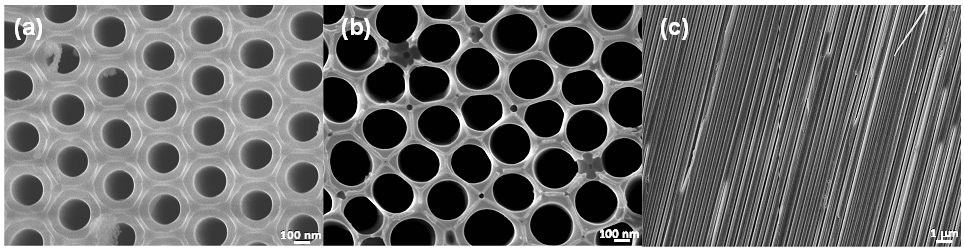

Figure 3. FEG-SEM views of RAAO membrane: (a) side A, (b) side B and (c) cross-section.

includes different sizes of pores (figure 1(b)), while the other side (side A —figure 1(a)) has irregularly shaped pores with an erratic interdistance.

Moreover, FEG-SEM cross-sectional views showed a low quality of the cutting plane (figure 1(c)), confirming that the porosity is not well ordered [41]. To sum up, the main geometrical characteristics of the Whatman commercial membranes (Anodisc 13 mm/0.2μm) are:

Pore mean diameter at side A: (273$\pm$48) nm (void fraction 30%).

Pore density at side A: 9×10^{12} pores m^{-2}.

Membrane thickness $\approx$60 μm.

3.1.2. Research membranes without thermal treatment. A specificity of the present study is the experimental removal of the compact layer of the supported AAO templates previously prepared [39, 40]. FEG-SEM plan views (figures 2(a) and (b)) revealed that this layer is progressively destroyed with increasing duration of the AC treatment. This removal is attributed to the gas evolution, especially during the cathodic part of the alternating waveform of the electrical signal.

At the end of the preparation process, FEG-SEM plan views (figures 3(a) and (b)) and cross-sectional view (figure 3(c)) of the AAO membranes (before thermal treatment) showed a well-defined microstructure. The pores are parallel, straight (figure 3(c)) and perpendicular to the initial metallic surface. In particular, the cutting plan is well-defined, proving the high quality of the porosity shape.

Furthermore, the pores are ordered, well formed and opened on both sides (figures 3(a) and (b)). However, there are differences between these two sides: the pore walls of side B are thinner but only 2–3 μm in depth. So the porosity of side A is the most representative of the whole membrane. The main characteristics of our RAAO membranes are:

Pore mean diameter at side A: (254$\pm$21) nm (void fraction 25%).

Pore mean diameter at side B: (285$\pm$25) nm (void fraction 48%).

Pore density at side A: 6.6×10^{12} pores m^{-2}.

Pore density at side B: 7.3×10^{12} pores m^{-2}.

Membrane thickness $\approx$60 μm.

Interdistance between the edges of two adjacent pores $\approx$200 nm.

Table 2. Global elementary composition of the AAO membranes, as obtained by EPMA.

Content	Oxygen (at.%)	Aluminium (at.%)	Phosphorus (at.%)
RAAO membrane (this study)	63.2 ± 1.4	36.1 ± 1.4	0.7 ± 0.1
CAAO membrane (200 nm)	60.8 ± 2.6	37.7 ± 2.5	1.5 ± 0.1
RAAO template with compact layer [39]	61.1 ± 1.4	36.3 ± 0.5	2.6 ± 0.2

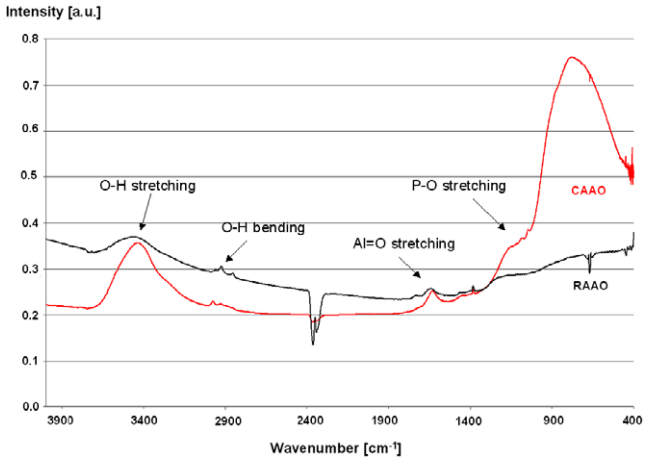

Figure 4. IR spectra of the CAAO and RAAO membranes prepared in KBr pellets.

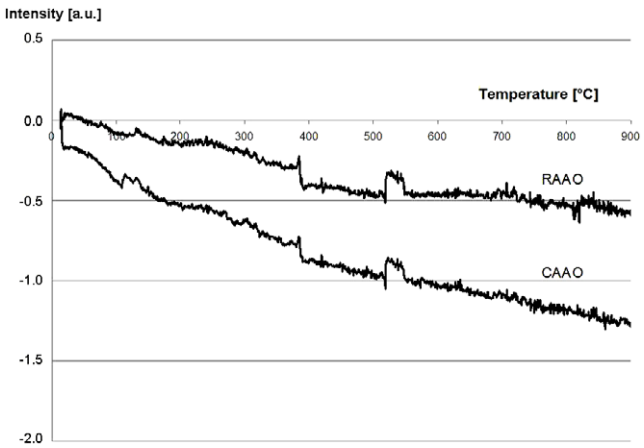

Figure 5. Thermogravimetric analyses of CAAO and RAAO membranes.

It is important to note that the pore density is similar on both faces, despite significant differences concerning the void fractions, confirming that the peculiarity of side B is only located at the extreme surface. Furthermore, the standard deviations of pore diameter are here low (<9%) for both faces in comparison with the value (about 18%) corresponding to side A of the commercial membranes.

3.1.3. Research membranes after thermal treatment. FEG-SEM plan views showed that the microstructure of the membrane remains unchanged despite a thermal treatment performed at 900 °C. On the other hand, a visual observation highlighted a bending phenomenon, i.e. that the membrane is curved after the thermal treatment. This result is in agreement with the works of Fernandez-Romero *et al* [42] using through-pores membranes prepared in an oxalic acid medium. The bending phenomenon appears significant in these two studies because there is no stabilizing effect of the barrier layer [42].

3.2. Chemical characterizations of the AAO membranes

3.2.1. Chemical composition. The global elementary composition of the AAO membranes was determined by EPMA (table 2).

Results showed no differences in the oxygen and aluminium atomic contents, while phosphorus content significantly changed. Phosphorus was included into the anodic films from the anodization electrolyte, using phosphoric acid. The difference of the phosphorus contents between the two types of RAAO membranes can be explained by the preferential acidic dissolution of the pore walls—including specifically phosphorus [40] during the additional removal of the compact layer. The explanation was corroborated by the comparison of the pore average diameter: (180 ± 30) nm and (254 ± 21) nm for the RAAO membranes, with and without compact layer, respectively.

Figure 4 shows the IR transmission spectra of typical RAAO and CAAO membranes, both types of samples being analysed in identical conditions. Both patterns had a similar shape, highlighting the O–H bond, Al=O double bond and P–O bond. However, the peaks corresponding to the RAAO membrane were undoubtedly lower than those of the CAAO sample, and lower than those of the AAO templates still including the compact layer [40].

To sum up, RAAO and CAAO membranes were chemically similar: before heating treatment both included hydrated (oxi)-hydroxide or oxide of aluminium, as well as phosphate coming from the anodization bath. But RAAO templates clearly showed a lower content of hydroxyl and phosphorus, due to the chemical dissolution of the pore walls during the removal of the compact layer.

3.2.2. Dehydration. Thermogravimetric analyses were performed in the 25–900 °C temperature range (figure 5) in order to study the dehydration mechanisms of RAAO and CAAO membranes. In accordance with previous works [40, 43], the sequence of weight changes was explained by the loss of physisorbed water (from 25 to 100 °C), and then of chemisorbed water in the 100–800 °C range. Finally, the total weight losses at 900 °C were 0.59% and 1.29% for RAAO and CAAO samples, respectively. So the weight losses were small, especially for the RAAO membrane, indicating low water content.

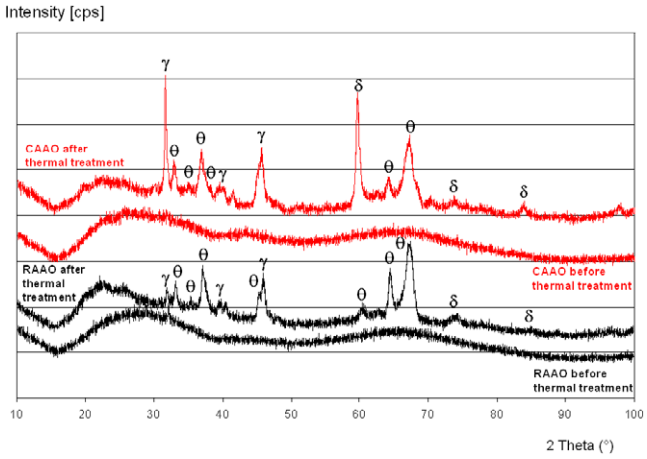

Figure 6. XRD spectra of CAAO and RAAO membranes before and after thermal treatment at 900 °C.

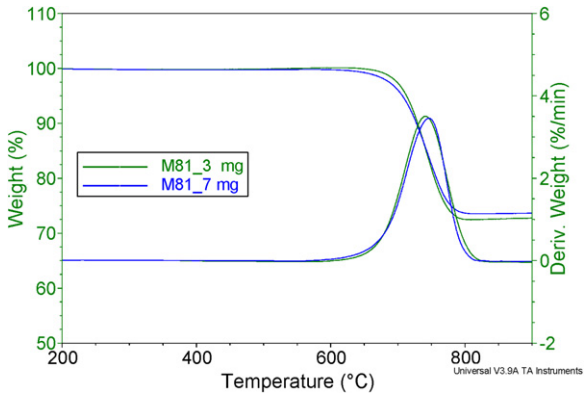

Figure 7. Thermogravimetrical analysis of M81 performed on two different mass weights for comparison.

3.2.3. Crystalline phase changes. Membranes were then studied by XRD as a function of temperature (25–900 °C) in order firstly to study the crystalline phase changes and secondly to contribute to understanding the subsequent formation of carbon nanotubes.

XRD spectra obtained just at the end of the preparation process showed only broad peaks (figure 6) for both research membranes and commercial ones. Therefore, both types of membranes were not made up of well-crystallized compounds but were in fact amorphous.

A thermal treatment was then performed at 900 °C in a nitrogen atmosphere to simulate the temperature used in the subsequent process of carbon growth. XRD spectra revealed (figure 6) the simultaneous presence of γ, δ and θ alumina crystalline phases, but without corundum (α-alumina).

These results are in agreement with previous works [40, 43], suggesting, in the 25–400 °C temperature range, dehydration mechanisms of physisorbed and chemisorbed water in the initial membrane, made up of aluminium hydrated (oxi)-hydroxide and then, at higher temperatures, the following successive crystallization phenomena:

$$2\mathrm{AlOOH} \rightarrow \gamma\text{-}\mathrm{Al_2O_3} + \mathrm{H_2O} \quad (1)$$

$$\gamma\text{-}\mathrm{Al_2O_3} \rightarrow \delta\text{-}\mathrm{Al_2O_3} \quad (2)$$

$$\delta\text{-}\mathrm{Al_2O_3} \rightarrow \theta\text{-}\mathrm{Al_2O_3}. \quad (3)$$

However, the present study showed that θ-alumina was surprisingly formed at temperature below 900 °C. Furthermore, comparison between the two types of membranes (RAAO and CAAO) clearly showed that the θ-alumina content is significantly higher in commercial membranes. This result can be perhaps explained by the difference in the respective phosphorus contents, i.e. (0.7 ± 0.1) at.% and (1.5 ± 0.1) at.%, respectively (table 2).

To sum up, our results showed that at 900 °C, i.e. the average temperature used in the subsequent process of carbon growth, AAO membranes were made up of crystallized allotropic alumina phases. Their respective contents depend on the previous anodization operational conditions and govern their respective catalytic activity, especially for the hydrocarbon decomposition and CNTs growth, due to their respective Lewis acid nature [31].

3.3. Characterizations of the CNTs/membrane composites

3.3.1. Thermogravimetric analysis (TG–DTG). To compare the effect of the operating conditions on the carbon structure order, thermogravimetric analyses [11–13] were performed on the samples reported in table 1. In fact, a different thermal behaviour, as shown by TG–DTG analysis, could contribute to characterize the carbon material present inside the pores with respect to its nature and structural order. The absence of catalyst particles, which in general could affect the carbon oxidation reaction, supports the validity of the result interpretation. To further validate such results, also considering the composite nature of samples, a preliminary test on different and very small sample weights (3–7 mg) was carried out to verify that the thermogravimetric profile was not affected by the weight of the sample (see figure 7 for M81). A final validation was carried out by first treating the composite sample by a thermal oxidation treatment up to an intermediate temperature value, reproducing the conditions of thermogravimetric analysis (see figure 8(b)) and then carrying out a thermogravimetric test on the residual mass. We have found the same temperature range of oxidation, indicating the same order degree for carbon (figure 8(c)).

In figure 9, the thermogravimetric profiles of M30 and M31 (obtained at the same operating conditions but except for reaction time) are shown. The comparison of TG–DTG profiles shows an higher carbon content for M30 as a result of the longer synthesis time. Moreover, for M30 an upshift of both endset and DTG peak temperature, indicating increased carbon order, is observed. For both samples the residual mass over 700 °C is that of the inorganic fraction, i.e. the AAO membrane.

For M31 and M32, prepared at the same operating conditions, except for ethylene concentration in the feed flow (table 1), TG–DTG analysis (figure 9(b)) indicates that a decrease in the ethylene concentration leads to the formation of a more ordered carbon structure. In particular, TG profiles exhibit one peak of weight loss; a comparison of the two

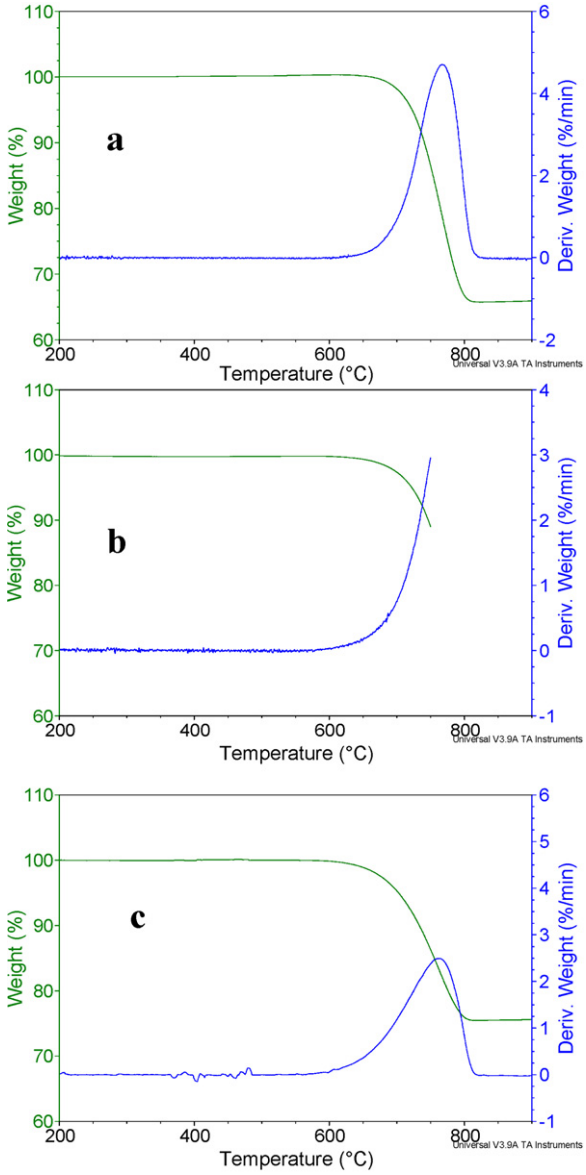

Figure 8. TG–DTG analysis of M78 (a), of M78 up to 745 °C (b) and on the M78 residue (c).

sample TG–DTG profiles shows that the oxidation results upshifted by about 50 °C for M32.

M30 and M60 differ only for the synthesis temperature, 100 °C higher in the case of M60. From the comparison of the onset and DTG peak temperature of the relevant profiles reported in figure 9(c) it can be concluded that the higher temperature synthesis results in (i) a more ordered carbon structure and (ii) a larger carbon content, likely due to a higher ethylene conversion, as the effect of temperature.

The effect of the reactor inlet total flow is shown in (figure 9(d)). The thermogravimetric profiles, relevant to M60 and M61, obtained at the same operating conditions except for total flow rate (the volume concentration of ethylene change remaining constant for the rate of ethylene fed), indicate that at an increased flow rate a more ordered carbon structure is achieved.

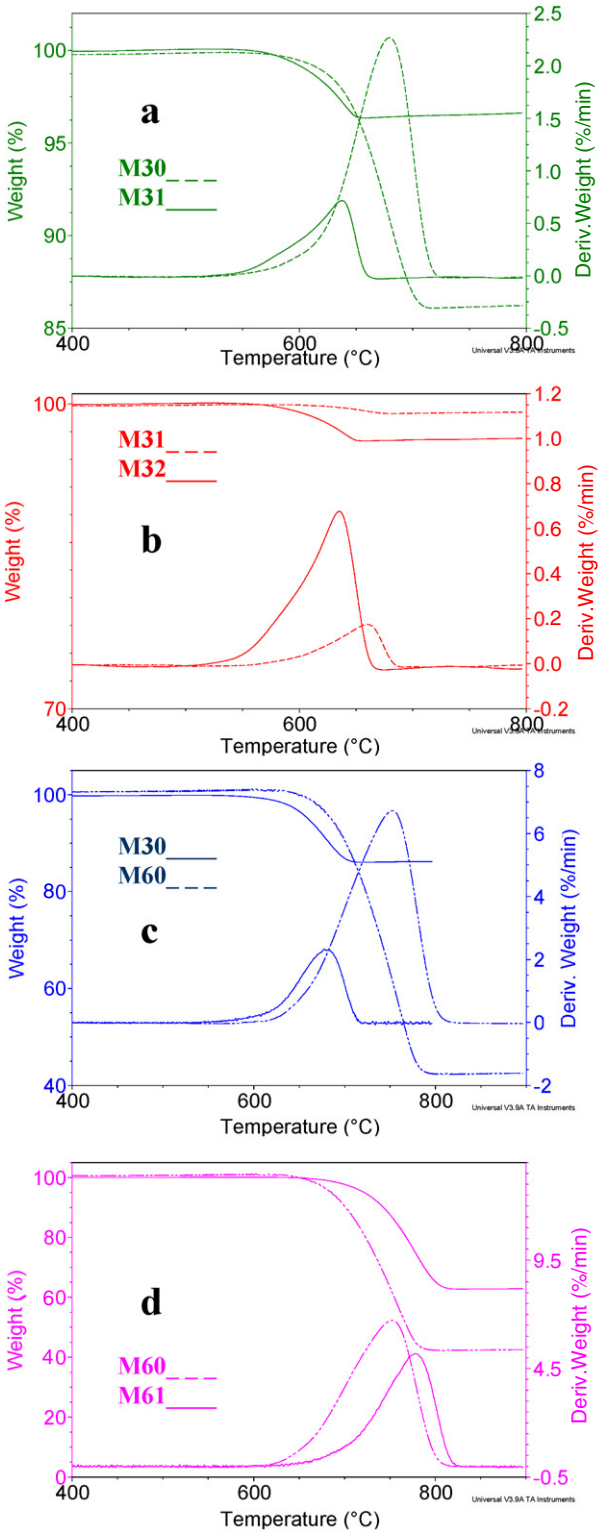

Figure 9. TG–DTG analysis to compare the effects: of time (a); of ethylene vol.% (b); of temperature (c) and of total feed flow (d) on the quality of the produced materials.

Figure 10 shows that in the range 25–800 °C the TG–DTG profiles of M29 (CAAO membrane) and M30 (AAO membrane) are practically superimposed. A single step weight loss, due to the combustion of the carbon material, is evident for both samples.

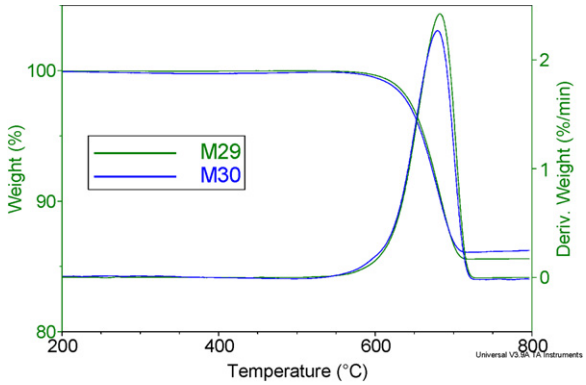

Figure 10. TG–DTG analysis to compare the syntheses in RAAO and CAAO membranes.

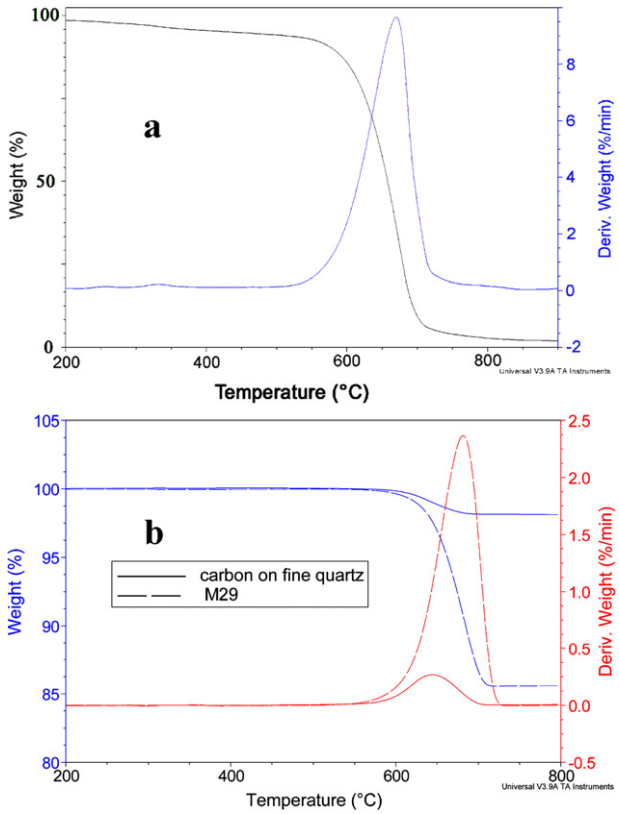

Figure 11. TG–DTG analysis on the CNT obtained after HF purification of M29 (a). TG–DTG of M29 and of the fine quartz, recovered from the reactor together with M29 (b).

In figure 11(a), the TG–DTG profile relevant to M29 after HF treatment to remove the membrane is shown: the residual mass due to alumina is quite close to zero.

Finally, to explore the catalytic effect of the membrane [31], giving our contribution to better understand its action, a test was performed in which the membrane together with an equal mass of fine quartz were loaded in the reactor in the same isothermal zone. After 30 min of the experiment, M29 and the quartz covered by carbon were collected from the reactor and subjected to two thermogravimetrical analyses for comparison (see figure 11(b)). Even if the onset of oxidation

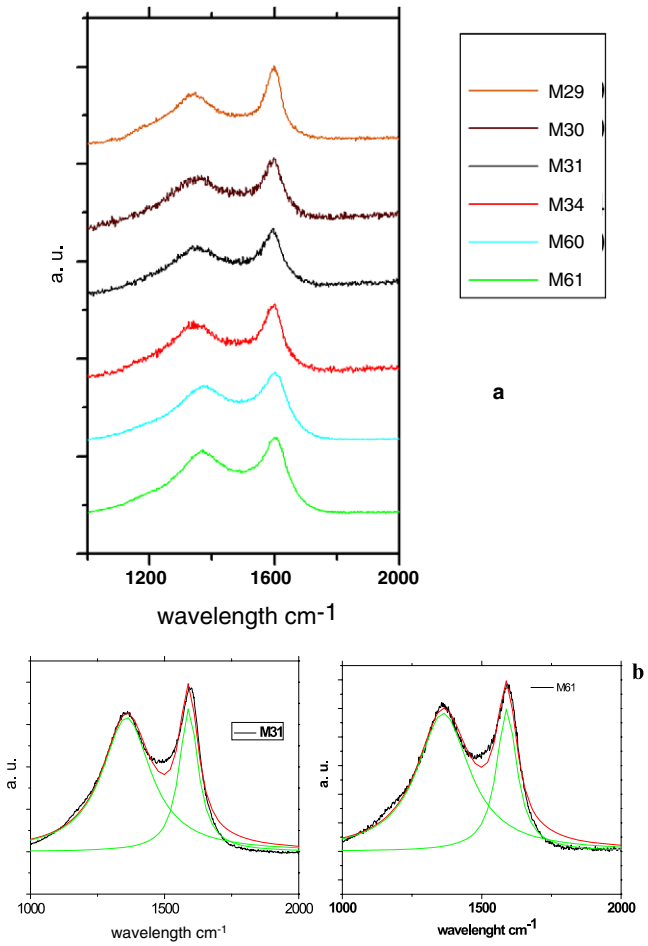

Figure 12. Raman spectra collected with 514 nm laser wavelength (a) and Lorentzian deconvolution of M31 and M61 Raman spectra (b).

seems to be quite close, the DTG peak and the endset of oxidation of M29 result in an upshift of about 40 °C, indicating the presence of different carbon contributions, some of which, in the case of M29, are more ordered.

Therefore, the formation of our carbon nanotubes is due to the combined effect of the catalytic behaviour of the internal alumina channels surface and their template effect, determining the formation of a carbon film that does not nucleate SWNTs [32–34] from the channel walls because of their smoothness.

3.3.2. Raman spectroscopy analysis. To confirm the results obtained with the TG–DTG evaluation the samples have been investigated by Raman spectroscopy analysis.

Raman spectra [13, 17], collected with a 514 nm laser wavelength, show the typical D and G peaks of the carbon materials, centred at about 1337 and 1599 cm^{-1}, respectively (figure 12(a)). The G peaks indicate the presence of crystalline graphite carbon, while the D peak can be attributed to amorphous carbon, defects in the curved graphene sheet and finite size of the tube crystalline domains. The fact that the two peaks have nearly identical magnitude indicates the presence of nanocrystalline graphite with domain size less than 10 nm [43].

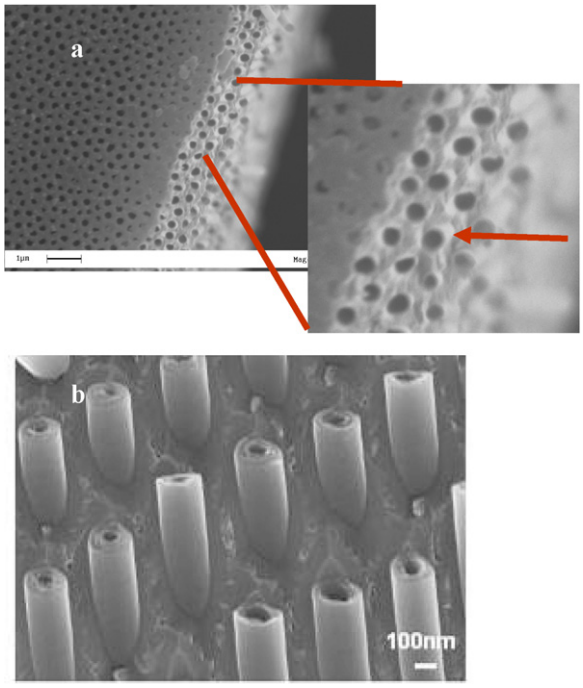

Figure 13. SEM images of the top surface and edge of M34, showing CNTs emerging from the RAAO channels (a). M29 CNTs from the alumina channels (b).

In table 3 the values of intensity ratio (I_D/I_G), which is a measure of the disorder amount, are reported. The values are not very different, from the largest one for M31 to the lowest ones for M61. Lorentzian deconvolution of M31 and M61 spectra (figure 12(b)) resulted in values of peak area ratio A_D/A_G in good agreement with the values of the intensity ratio (table 3).

Table 3. Raman characterization results.

Sample	I_D/I_G	A_D/A_G
M29	0.76	
M30	0.76	
M31	0.78	2.5
M34	0.77	
M60	0.73	
M61	0.72	2.4

Raman spectroscopy results are in accordance with those from TG–DTG analysis, confirming that carbon order increases by increasing synthesis time, total feed flow, temperature and decreasing ethylene concentration.

3.3.3. SEM and TEM microscopy. Figure 13(a) shows the top surface and edge of composite M34: CNTs can be seen to emerge from pores on the membrane edge. Figure 13(b) shows the CNTs emerging from the AAO membrane after 30 min of synthesis at 850 °C (sample M29). The images clearly show the growth of carbon tubes, one tube for each channel. The external diameter of the tubes is uniform and close to the membrane pore diameter.

The dissolution of the membrane results in bundles of parallel tubes, opened and aligned (due to van der Waals interaction among the bundle), without microscopic defects. The bundles of aligned CNT are as long as the thickness of the original membrane (sample M29 in figure 14). There is no significant evidence of any amorphous carbon (figure 15). The images in figure 15(c) are the SAD patterns taken in the selected area indicated by a circle in figure 15(b). In the image a pair of arcs for 002, together with 10 and 11, diffraction rings is hardly visible. The appearance of the 002 diffraction neither as a ring nor as clear spots, but as a pair of arcs, indicates some orientation of the 002 planes in the carbon tubes and

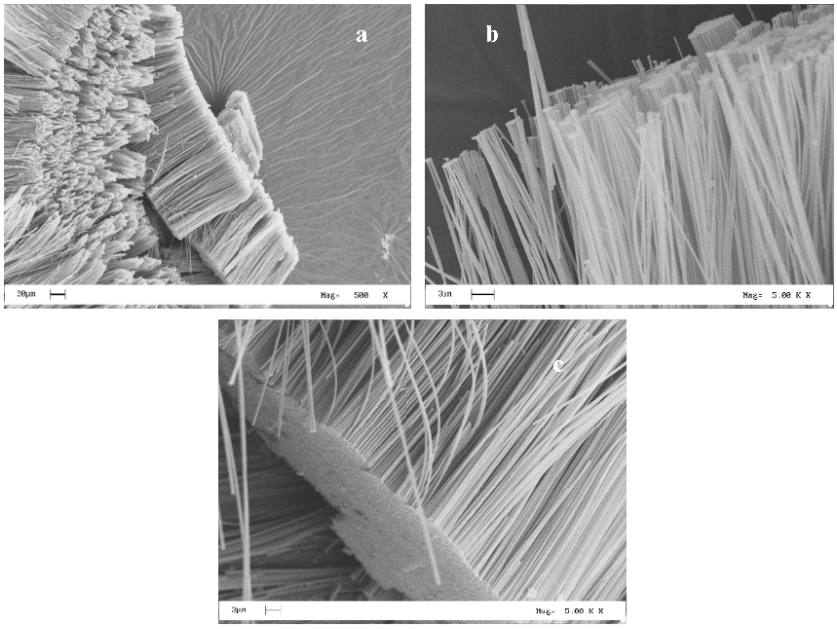

Figure 14. SEM images of M29 CNT bundles, after HF dissolution of the membrane, at different magnifications.

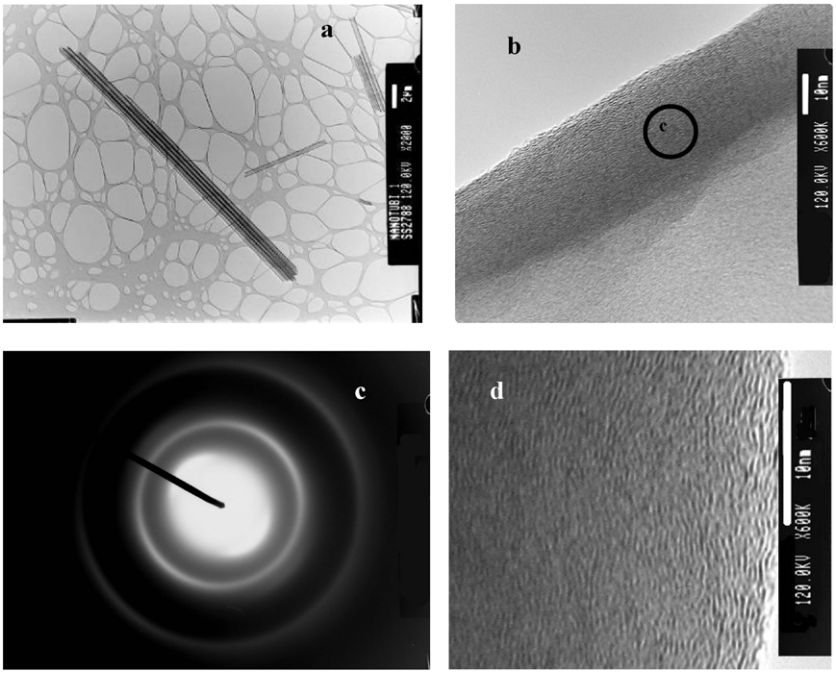

Figure 15. CNT bundle grown in the channels of RAAO membrane, after dissolution of the membrane in M29, TEM images at different magnifications (a), (b), (d); SAD pattern (c).

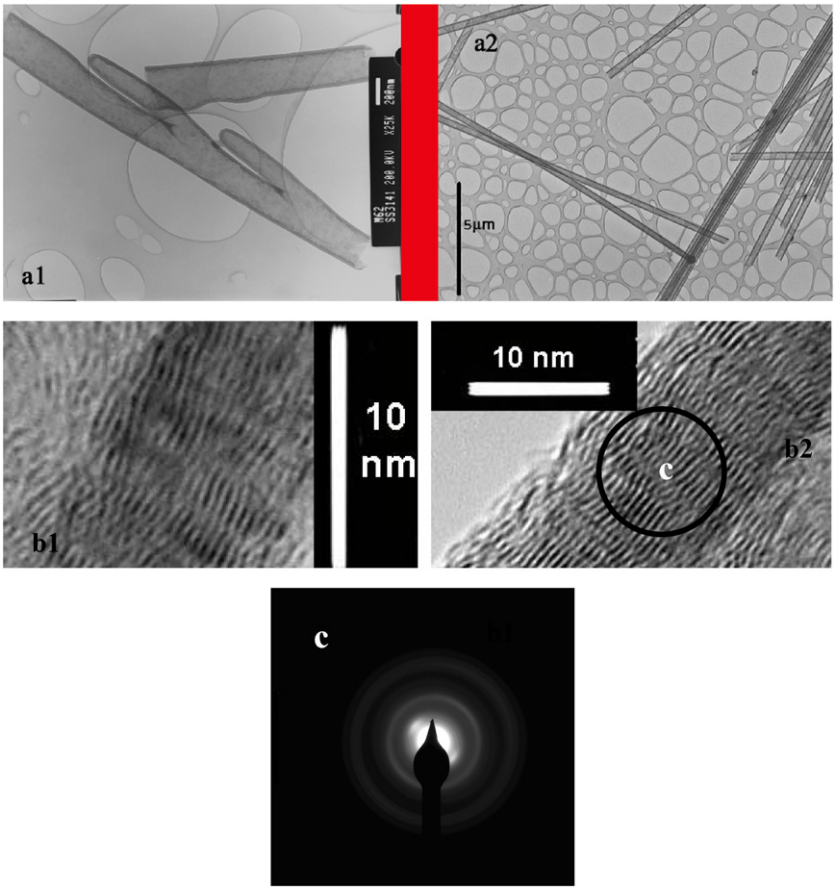

Figure 16. TEM–HRTEM images of CNTs produced in the channels: of CAAO membrane (M81) at lower (a1) and higher magnification (b1); of RAAO membrane (M144) (a2) and at higher magnification (b2). SAD pattern taken in area c of image b2 (c).

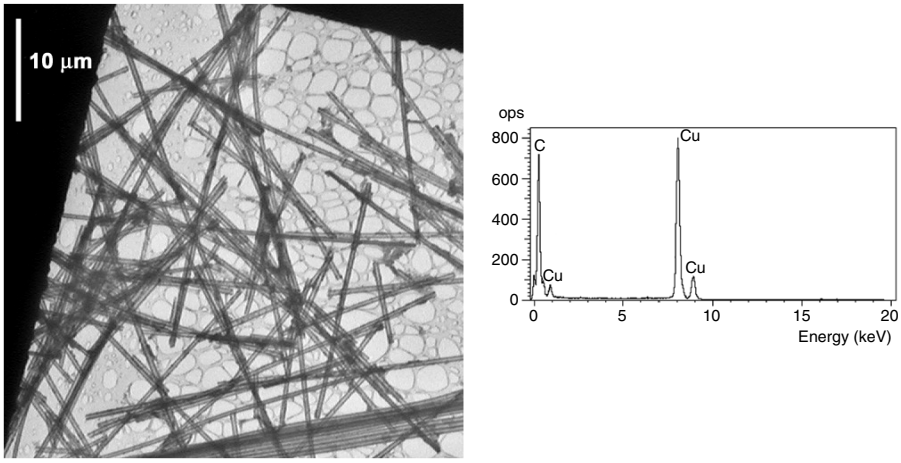

Figure 17. TEM images of CNTs produced in the channels of M29 (the black area are due to the TEM grid). EDX spectrum taken in the image area.

its poor crystallinity. For this carbon tube, the SAD patterns, taken from areas that do not contain the edge of the tubes, do not show the 002 arc, since in this area no beam passed through the tube wall in parallel as in area c. This finding suggests that the tube wall consists of cylindrically stacked 002 planes [7]. Higher magnification TEM characterization permits us to observe the carbon arrangement in the tube thickness: twisted walls are observed in the direction of the nanotube axis (figure 15(d)).

With respect to the shape and morphology of the nanotubes, they reflect the shape and morphology of the membrane, resulting in more ordered bundles of straight nanotubes with uniform size in the channels of the RAAO membrane (compare figures 16(a1) and (a2)). Higher magnifications (figures 16(b1) and (b2)) indicate that the twisted walls in the direction of the nanotubes axis are more ordered (more straight and with less interruptions) if compared with those of figure 15(d). The image in figure 16(c) is the SAD pattern taken in the selected area indicated by the circle in figure 16(b2), it exhibits a pair of smaller and stronger arcs for 002, together with 10 and 11, diffraction rings, indicating a better degree of order for this nanotube, in agreement with thermogravimetric and Raman characterizations. The purity of the produced CNTs after HF alumina removal is shown by the EDX analysis, performed on a large area, showing the presence of the peaks due to the carbon nanotubes and the TEM grid (figure 17).

4. Conclusions

This study showed that both RAAO and CAAO initially include hydrated (oxi)-hydroxide or oxide of aluminium, as well as phosphate coming from the anodization bath. However, RAAO templates include lower contents of water and phosphorus and show a better porosity shape.

After thermal treatment, RAAO membranes were made up of crystallized allotropic alumina phases, which govern the subsequent CNT growth, because of their catalysis activity, likely due to their respective Lewis acid natures.

CNTs were then grown by chemical vapour deposition (CVD), in the absence of metallic catalyst, in the pores of both CAAO and RAAO membranes. A composite material, containing one nanotube for each channel, having the same length as the membrane thickness and an external diameter close to the diameter of the membrane holes, was obtained. SEM and TEM images of the samples after HF removal of alumina show the formation of bundles of parallel tubes, opened and aligned without macroscopic defects. The shape and morphology of the nanotubes reflect the shape and morphology of the membrane; more ordered bundles of straight nanotubes with uniform size in the channels were obtained for RAAO membranes.

The carbon structure order depends on the CVD experimental conditions: it is increased by increasing synthesis time, total feed flow rate and reaction temperature, and decreasing ethylene concentration.

Acknowledgment

This work has been performed within the European research project CATHERINE—Carbon nAnotube Technology for High-speed nExt-geneRation nano-InterconNEcts—under grant agreement no. 216215.

References

[1] Suh J S, Jeong K S, Lee J S and Han I 2002 *Appl. Phys. Lett.* **80** 2392
[2] Li J, Stevens R, Delzeit L, Ng H T, Cassell A, Han J and Meyyappan M 2002 *Appl. Phys. Lett.* **81** 10
[3] Gao H, Mu C, Wang F, Xu D, Wu K, Xie Y, Liu S, Wang E, Xu J and Yu D 2003 *J. Appl. Phys.* **93** 5602
[4] Pribat D, Cojocaru C S, Gowtham M, Marquardt B, Wade T, Wegrowe J E and Kim B S 2009 *C. R. Phys.* **10** 320
[5] Jung H Y, Jung S M and Suh J S 2008 *Carbon* **46** 1345
[6] Yoon S M, Chae J and Suh J S 2004 *Appl. Phys. Lett.* **84** 825
[7] Kyotani T, Tsai L F and Tomita A 1996 *Chem. Mater.* **8** 2109
[8] Che G, Lakshmi B B, Martin C R and Fisher E R 1998 *Chem. Mater.* **10** 260

[9] Vermisoglou E C, Pilatos G, Romanos G E, Karanikolos G N, Boukos N, Mertis K, Kakizis N and Kanellopoulos N K 2008 *Microporous Mesoporous Mater.* **110** 25
[10] Yap H Y, Ramaker B, Sumant A V and Carpick R W 2006 *Diamond Relat. Mater.* **15** 1622
[11] Ciambelli P, Sannino D, Sarno M, Fonseca A and Nagy J B 2004 *J. Nanosci. Nanotechnol.* **4** 779
[12] Ciambelli P, Sannino D, Sarno M, Fonseca A and Nagy J B 2004 *Adv. Eng. Mater.* **6** 804
[13] Scheneider J J, Maksimova N I, Engstler J, Joshi R, Schierholz R and Feile R 2008 *Inorg. Chim. Acta* **361** 1770
[14] Sang J and Lee J S 1999 *Appl. Phys. Lett.* **75** 2047
[15] Yuan Z H, Huang H, Liu L and Fan S S 2001 *Chem. Phys. Lett.* **345** 39
[16] Zhang X Y, Zhang L D, Zheng M J, Li G H and Zhao L X 2001 *J. Cryst. Growth* **223** 306
[17] Kim M J, Lee T Y, Choi J H, Park J B, Lee J S, Kim S K, Yoo J B and Park C Y 2003 *Diamond Relat. Mater.* **12** 870
[18] Lee O J, Hwang S K, Jeong S H, Lee P S and Lee K H 2005 *Synth. Met.* **148** 263
[19] Ding D, Chen Z, Rajaputra S and Singh V 2007 *Sensors Actuators* B **124** 12
[20] Sklar G P, Paramguru K, Misra M and LaCombe J C 2005 *Nanotechnology* **16** 1265
[21] Chen P L, Chang J K, Kuo C T and Pan F M 2005 *Appl. Phys. Lett.* **86** 123111
[22] Jeong S H, Hwang H Y, Hwang S K and Lee K H 2004 *Carbon* **42** 2073
[23] Tu J P, Jiang C X, Guo S Y and Fu M F 2004 *Mater. Lett.* **58** 1646
[24] Jeong S H, Lee O J and Lee K H 2002 *Chem. Mater.* **14** 1859
[25] Suh J S and Lee J S 1999 *Appl. Phys. Lett.* **75** 2047
[26] Sui Y C, Cui B Z, Guardian R, Acosta D R, Martinez L and Perez R 2002 *Carbon* **40** 1011
[27] Sui Y C, Acosta D R, Gonzalez-Leon J A, Bermudez A, Feuchtwanger J, Cui B Z, Flores J O and Saniger J M 2001 *J. Phys. Chem.* B **105** 1523
[28] Rummeli M H, Kramberger C, Gruneis A, Ayala P, Gemming T, Buchner B and Pichler T 2007 *Chem. Mater.* **19** 4105
[29] Oya A and Marsh H 1982 *J. Mater. Sci.* **17** 309
[30] Lee J S, Gu G H, Kim H, Jeong K S, Bae J and Suh J S 2001 *Chem. Mater.* **13** 2387
[31] Scokart P O and Rouxhet P G 1982 *J. Colloid Interface Sci.* **86** 96
[32] Huang S, Cai Q, Chen J, Qian Y and Zhan L 2009 *J. Am. Chem. Soc.* **131** 2094
[33] Homma Y, Liu H, Takagi D and Kobayashi Y 2009 *Nano Res.* **2** 793
[34] Liu H, Takagi D, Ohno H, Chiashi S, Chokan T and Homma Y 2008 *Appl. Phys. Express* **1** 014001
[35] Sui Y C, Gonzales-Leon J A, Bermudez A and Saniger J M 2001 *Carbon* **39** 1709
[36] Delpeux-Ouldriane S, Szostak K, Frackowiak E and Béguin F 2006 *Carbon* **44** 799
[37] Hornyak G L, Dillon A C, Parilla P A, Schneider J J, Czap N, Jones K M, Fasoon F S, Mason A and Heben M J 1999 *Nano Struct. Mater.* **12** 83
[38] Che G, Lakshmi B B, Fisher E R and Martin C R 1998 *Nature* **393** 346
[39] Le Coz F, Arurault L, Fontorbes S, Vilar V, Datas L and Winterton P 2010 *Surf. Interface Anal.* **42** 227
[40] Le Coz F, Arurault L and Datas L 2010 *Mater. Charact.* **61** 283
[41] Arrowsmith D J, Clifford A W and Moth D A 1986 *J. Mater. Sci. Lett.* **5** 921
[42] Fernandez-Romero L, Montero-Moreno J M, Pellicer E, Peiro F, Pellicer E, Peiro F, Cornet A, Morante J R, Sarret M and Müller C 2008 *Mater. Chem. Phys.* **111** 542
[43] Tunistra F and Kocing J L 1970 *J. Phys. Chem.* **53** 1126